ISSN 1023-1935, Russian Journal of Electrochemistry, 2015, Vol. 51, No. 8, pp. 712–718. © Pleiades Publishing, Ltd., 2015.
Published in Russian in Elektrokhimiya, 2015, Vol. 51, No. 8, pp. 805–812.

Facile Synthesis Cuboid SnO_2 Nanoparticles and Electrochemical Properties as Anode of Lithium-Ion Battery[1]

Pei-Pei Dong, Yan-Hui Sun[z], Xu Lang, Jun-Min Nan, and Hong-Yu Chen

School of Chemistry and Environment, South China Normal University, Guangzhou 510006, P. R. China

Received October 11, 2013

Abstract—SnO_2 nano-cuboids were synthesized by a simple precipitate of $SnCl_2$ in oxalic acid and followed by temperature—controlled decomposition of $Sn_2C_2O_4$ annealing in air. SEM, TEM and X-ray diffraction showed that the products are uniformly nano-cuboids with the size around 40 nm in width, 100 nm in length and 10 nm in height in rutile phase. The electrochemical performances of the nano-cuboids were tested by galvanostatically discharge/charge, cyclic voltammetry. The initial discharge and charge capacities reached 2410 and 1468 mA h g^{-1} and maintained 915 and 859 mA h g^{-1} after 30 cycles at 0.1 C. The discharge capacity still kept at 418 mA h g^{-1} after 30 cycles at 0.2, 0.5, 1, 2 and 0.2 C. The perfect reversibility and cycling stability of the cell was contributed to the smaller nanosize of cuboid SnO_2. Moreover, the mechanism of SnO_2 anodes undergoing the conversion of Sn to SnO and then SnO_2 along with alloying of Li_xSn enabled higher capacity was verified by XRD and CV measurements.

Keywords: SnO_2, cuboid nanoparticles, anode, lithium-ion battery, electrochemical performances

DOI: 10.1134/S1023193515080042

1. INTRODUCTION

SnO_2 has been considered as a promising anode material for lithium-ion batteries (LIBs) due to its low cost, safety and especially high theoretical capacity compared with the carbon material (with a theoretical capacity of 372 mA h g^{-1}) [1–3]. Therefore SnO_2-based materials have attracted great interest as promising substitutes for the commercial graphite anodes. Unfortunately, pure SnO_2 surfers from a large volume change during lithium alloying and de-alloying, and this would induce huge internal stress in the electrode material, which leads to disintegration and loss of electric contact, and eventually results in quick capacity fading upon extended cycling [4–10].

Different strategies have been proposed to resolve the above mentioned problems of SnO_2-based anodes. One effective way is to create uniquely nanostructured SnO_2 and the other approach is to introduce carbonaceous materials into the SnO_2 electrodes [11–15]. In this regard, various SnO_2 nanostructures, such as nanotubes [4], nanosheets [5], hollow nanospheres [6], nanowire [7], nanobelts [8] and nanorods [9] have been investigated as anode materials for LIBs. These anode materials have been proved to minimize the severe volume change and exhibit better electrochemical performance, suggesting that structure modification could be a good solution to the poor cyclic retention of SnO_2-based anode materials [10].

On the other hand, Idoda et al. [3] first suggested SnO_2 as anode materials for LIBs in 1997. They believed that lithium can be reversibly stored in SnO_2 ($SnO_2 + xLi^+ + xe = Li_xSnO_2$). Later Liu et al. [16] showed that SnO_2 is irreversibly reduced to Li_2O and metallic Sn in the initial discharge ($SnO_2 + 4Li^+ + 4e \longleftrightarrow Sn + 2Li_2O$). This explained the low initial coulombic efficiency of SnO_2, which is one of the major obstacles to its commercial application. Courtney and Dahn [17] further proved that the lithium storage in SnO_x is by Li_xSn alloying and de-alloying ($Sn + xLi^+ + xe \longleftrightarrow Li_xSn$, $0 \le x \le 4.4$). They proposed that the theoretical lithium storage capacity of Sn by the Li_xSn alloying is 991 mA h g^{-1}, more than twice the theoretical capacity of commercial graphite carbon. Both of the above reactions have been well accepted and become the basis for evaluating the electrochemical performances of SnO_2 anodes [4, 6, 18–20]. Recently, the mechanism that the theoretical capacity of Sn based compounds is voltage controlled process was proposed [21–23]. As the upper cut-off potential of <0.8 V vs. Li, the theoretical capacity is 782 mA h g^{-1}, which corresponds to the alloying/de-alloying of $Li_{4.4}Sn$. Upper cut-off potential of 0.8–1.65 V vs. Li, the corresponding theoretical capacity is 1138 mA h g^{-1}, (metallic Sn particles subsequently were oxidized to SnO, which uptakes of maximum 6.4 moles of Li); and at potential window exceeding 1.65 V vs. Li, the consequent oxidation of Sn^{2+} (SnO) in to Sn^{4+} (SnO_2) happened, which uptakes of

[1] The article is published in the original.

[z] Corresponding author: sunyanhui0102@163.com (Yan-Hui Sun).

maximum 8.4 moles of Li with corresponding theoretical capacity of ~1494 mA h g^{-1}) [21]. Above mechanism was proposed based on the CV spectra and theoretical analysis, and this interesting point waits further verifying in SnO_2 electrodes with novel nanostructure.

In this study, SnO_2 nanoparticles with a new cuboid morphology were synthesized by a simple precipitate of $SnCl_2$ with $H_2C_2O_4 \cdot 2H_2O$ following by temperature—controlled decomposition of $Sn_2C_2O_4$ annealing in air. The electrochemical properties of the SnO_2 nano-cuboids display superior lithium-ion storage performance with very large initial discharge and charge capacities and high coulombic efficiency, excellent cyclic performance and good rate capability. We verified the conversion reaction of Sn to SnO and then SnO_2 along with the Li_xSn alloying reaction enables the higher charge/discharge capacity of SnO_2 anode by cyclic voltammetry spectra and XRD determination of the anode materials after cycling.

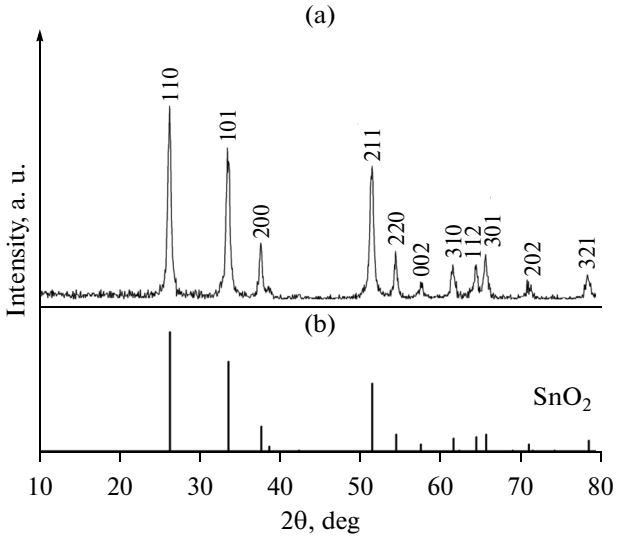

Fig. 1. XRD patterns of (a) as-prepared SnO_2 samples after annealing at 350°C in air for 2 h; (b) standard diffraction patterns of SnO_2.

2. EXPERIMENTAL SECTION

2.1. Synthesis of SnO_2 Nano-Cuboids

The experimental procedure for the synthesis of SnO_2 nano-cuboids can be described as follows: 0.21 g $H_2C_2O_4 \cdot 2H_2O$ was dissolved in 50 mL of de-ionized water. After magnetic stirring for 5 min, a transparent solution was obtained, then 0.4 g $SnCl_2 \cdot 2H_2O$ was directly added into the above solution at once time without stirring, and the white pine—tree branches crystal precipitate generated immediately. Aging for 30 min, the white precipitates were separated by centrifugation at 4500 rpm for 20 min and dried at 60°C for 20 h in air. The dried precursors were shifted into a muffle furnace, which was controlled at the heating rate of 3°C min^{-1} and annealed at 350°C for 2 h, and then naturally cooled down to room temperature. Finally, the light-gray product was obtained.

2.2. Characterization of the Synthesized Materials

Structural characterization of the prepared sample was performed by means of X-ray diffraction (XRD, Model Y2000, China) with Cu$K\alpha$ radiation (λ = 1.5406 Å), at 30 kV and 20 mA. The structure and morphology of the products were observed using a scanning electron microscope (SEM, Model ZEISS Ultra 55, Germany) and transmission electron microscope (TEM, Model JEM-2100HR, Japan).

2.3. Electrochemical Characterization of SnO_2 Nano-Cuboids as Anode of LIBs

Electrochemical characterization was performed in the form of CR2025 coin-type lithium half cells, in which the prepared SnO_2 as the working electrode (anode) and the lithium (Li) foil was used as a counter (cathode) and reference electrode. The working electrode was prepared by mixing the active material (SnO_2 1.5 mg), acetylene black and polyvinylidene fluoride (PVDF) with a weight ratio of 80 : 10 : 10, and pasted on a copper foil with 18 μm thickness as a current collector. Then the electrode was dried at 100°C for 15 h in a vacuum oven. The electrolyte was prepared by dissolving 1 M $LiPF_6$ in ethylene carbonate (EC) and dimethyl carbonate (DMC) with a volumetric ratio of 1 : 1. A layer of Celgard 2025 (Celgard, Inc., USA) porous membrane was used as a separator. The cell was assembled in a glove box under argon atmosphere where both the moisture and oxygen contents were below 1 ppm. The cells were galvanostatically charge–discharged in the voltage range 0–2.5 V vs. Li/Li^+ at different current rates between 0.1 and 2 C (1 C rate corresponds to the current density of 782 mA g^{-1}) via a Battery Testing System (Neware Technology Limited, CT-3008W-5V1mA-S4, China). The cyclic voltammetry (CV) measurements were recorded between 0 and 3 V (vs. Li/Li^+) at scan rate of 0.1 mV s^{-1} using a CHI 660A electrochemical workstation.

3. RESULTS AND DISCUSSION

3.1. Microstructure and Morphology of Synthesized SnO_2 Sample

XRD patterns of as-prepared SnO_2 sample after annealing at 350°C in air for 2 h are showed in Fig. 1a. All the diffraction peaks in XRD patterns can be well indexed with the tetragonal rutile phase of SnO_2, which is confirmed by a comparison with the standard diffraction peaks (JCPDS 41-1445) in Fig. 1b. It can be seen that no impurity peaks are observed indicating the high purity of the prepared products. The peak

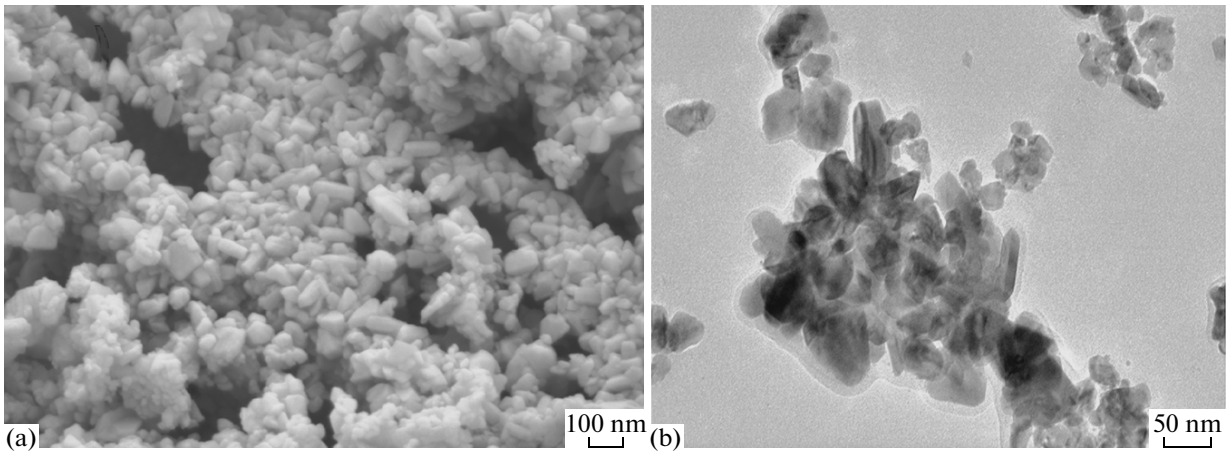

Fig. 2. (a) SEM image and (b) TEM image of the synthesized SnO_2 nanoparticles.

intensities of (110), (101) and (211) planes are sharper than the peaks of other crystal planes, which means nano-cuboid of SnO_2 crystals mainly grow along the three planes at 350°C. The average crystalline size of the SnO_2 is calculated to be about 15 nm according to the Debye–Scherrer formula.

Figure 2 shows the morphology of the synthesized SnO_2 by SEM and TEM images, respectively. The SEM image in Fig. 2a reveals that SnO_2 presented as regular cuboid with about 40 nm in width and 100 nm in length and with a little aggregation. It can be seen from TEM image in Fig. 2b, the cuboid particles show about 10 nm in height, and there are some irregular shapes of SnO_2. The size of the nano-cuboid is different from that calculated from the XRD patterns, which is attributed to the calculated size based on Debye–Scherrer formula is an average of each crystal plane.

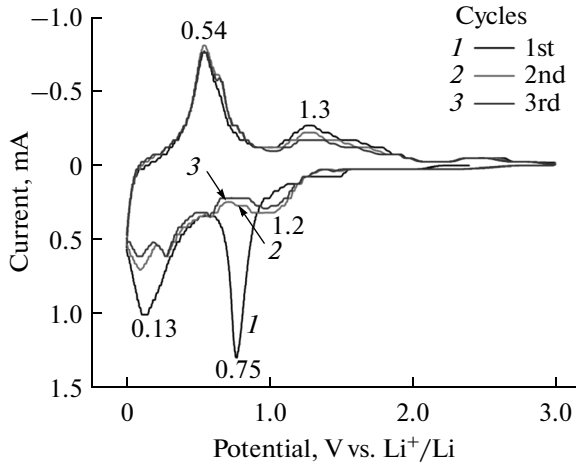

Fig. 3. CV curves of the cuboid SnO_2 nanopartiecles at a scan rate of 0.1 mV s^{-1}.

3.2. Electrochemical Properties of the SnO_2 Nano-Cuboids

To better determine the electrochemical reaction and reversibility of SnO_2 electrode, cyclic voltammetry (CV) measurements are carried out. Figure 3 shows the CV curves of SnO_2 in the first three scanning cycles at 0.1 mV s^{-1} in the range of 0–3.0 V. In the first cycle, there is a strong cathodic peak around 0.75 V (vs. Li^+/Li) that occurs from the reduction of SnO_2 to Sn and formed Li_2O by consuming Li^+ in electrolyte as given by Eq. (1) and the formation of a solid electrolyte interphase (SEI) film by Eq. (2) [19–23]. SEI formation is caused by the decomposition of the electrolyte and the lithium salt at the surface of the electrode, and this peak (0.75 V vs. Li^+/Li) disappears after the first cycle. Whether the SEI film can be formed in the next cycles is related to the surface of the anode material. Kilibarda et al reported that the reduction peak was repeated in the second and third cycles because during lithiation and delithiation some parts of this film may break off that resulted the fresh surface of active material gets into contact with the electrolyte, new SEI formation takes place as long as required additives in the electrolyte are not completely consumed [24–27].

$$SnO_2 + 4Li^+ + 4e \longleftrightarrow Sn + 2Li_2O. \quad (1)$$

$$\text{Electrolyte} + xLi^+ + xe \longrightarrow \text{SEI layer}. \quad (2)$$

$$Sn + xLi^+ + xe \longleftrightarrow Li_xSn \quad (0 \le x \le 4.4)(<0.8\ \text{V vs. Li}). \quad (3)$$

$$2Sn + Li_2O \longleftrightarrow 2SnO + 2Li^+ + 2e \quad (>0.8\ \text{V vs. Li}). \quad (4)$$

$$SnO + Li_2O \longleftrightarrow SnO_2 + 2Li^+ + 2e \quad (>1.65\ \text{V vs. Li}). \quad (5)$$

The other intensive cathodic peak is around 0.13 V (vs. Li^+/Li), corresponds to the formation of Li_xSn

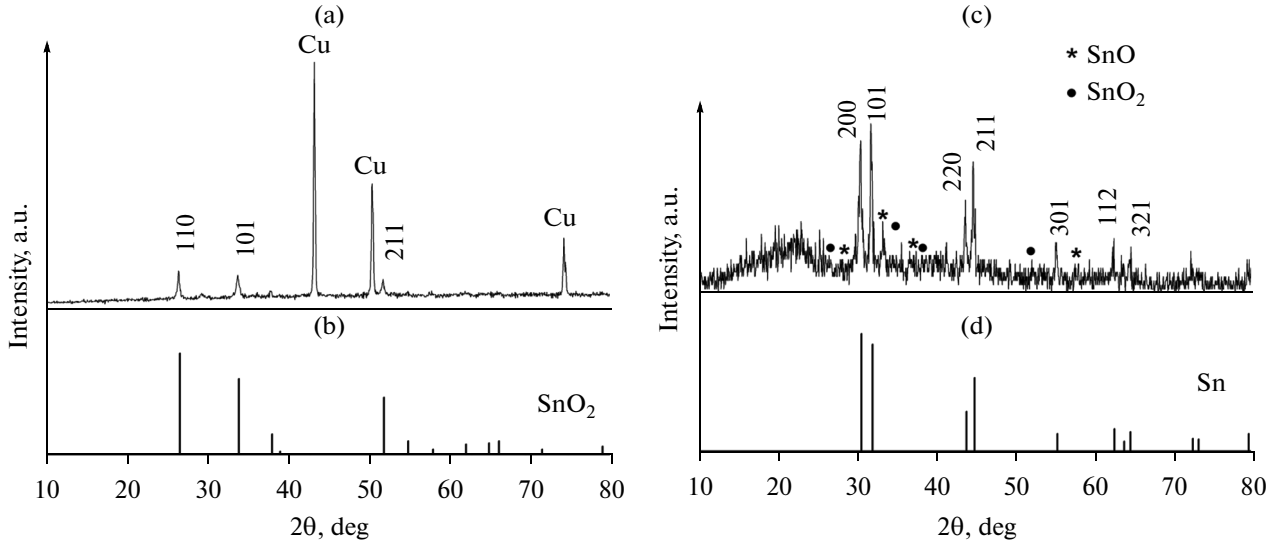

Fig. 4. XRD patterns of (a) working electrode composed of SnO_2 materials coated on Cu foil with PVDF, NMP and acetylene black; (b) standard diffraction peaks of SnO_2; (c) the 16 times—cycled SnO_2 nanoparticles disassembled in a glove box, washed in acetone and dried in vacuum; (d) standard diffraction peaks of Sn.

alloys (Li_2Sn_5, LiSn, Li_7Sn_3, Li_5Sn_2 and $Li_{22}Sn_5$) as described in Eq. (3). In the anodic curve, the peak at 0.54 V (vs. Li^+/Li) can be attributed to Li de-alloying from Li_xSn and formed metallic Sn according to Eq. (3). There is a weak oxidation peak of 1.3 V, and the attribution of this peak has two views, one is the traditional understanding of partly reversible reaction (Eq. (1)) from Sn into SnO_2 [28–30] as described in Eq. (1), and another one is the oxidation of metallic Sn to SnO, based on Eq. (4) (maximum uptake of 6.4 moles of Li with corresponding theoretical capacity of ~1138 mA h g^{-1}) [21–23]. According to the later view, potential window exceeding 1.65 V vs. Li enables the consequent oxidation of Sn^{2+} (SnO) in to Sn^{4+} (SnO_2, maximum uptake of 8.4 moles of Li with corresponding theoretical capacity of ~1494 mA h g^{-1}) as shown in Eq. (5). But no oxidation peaks exceeds 1.65 V vs. Li were observed in this study, which maybe due to the faster scan rate of 0.1 mV s^{-1} in this study and 50 μV s^{-1} in reference [21] in CV measurements. Many literatures did not study the mechanism of Eqs. (4) and (5) because the CV scan rate was too fast and could not determine these oxidation peaks in CV curves [28–31].

In the second and third cycles, the reduction peak at 0.75 V (vs. Li^+/Li) disappeared and showed the broad reduction peak at about 1.2 V (vs. Li^+/Li). According to the traditional view [31], the broad reduction peak of 1.20 V, together with the oxidation peak about 1.3 V, suggesting partial reversibility of the reduction of SnO_2 to Sn (Eq. (1)). Another view indicated that the reduction peak at 1.2 V should attribute to the reduction of SnO to metallic Sn based on Eq. (4), while the oxidation peak at 1.3 V attribute to the reversible reaction from Sn to SnO. The fact that SnO phase exists in the anode materials after cycling confirmed the later view is reasonable [21–23]. The reversible extent of Eq. (4) in the second and third cycles is much higher than that in the first cycle (the ratio of current peak is near to 1 at redox-couple at 1.2 and 1.3 V). The other reduction peaks located between 0.75 and 0 V, together with the oxidation peak at 0.54 V correspond to the alloying and de-alloying of Li_xSn [28] as described in Eq. (3). But no oxidation peaks exceeds 1.65 V vs. Li were observed yet in the second and third cycles. What's more, the CV profiles of the second and the third cycle almost overlap, in support of the reversibility of the electrochemical reaction in the anode of Li-ion batteries as well.

It can be seen that the alloying/de-alloying reaction of Li_xSn seems to be partially—reversible resulted from that the ratio of peak current of cathodic and anodic is not equal to 1 involved in the charging and discharging process (redox-couple at ~0.13 and 0.54 V), and the Eq. (4) is partly reversible too for the ratio of peak current of cathodic and anodic is not equal to 1 (redox-couple at 1.2 and 1.3 V). The unbalanced behavior of discharge and charge resulted in irreversible capacity loss in the following cycles.

To further investigate the SnO_2 anode undergoes the conversion reaction along with alloying reaction mechanism mentioned above, the SnO_2 working electrode after 16 cycles was analyzed by XRD, and as a comparison, the new working electrode composed of SnO_2 material coated on Cu foil with PVDF, NMP and acetylene black was analyzed by XRD too, and the results are showed in Fig. 4. In Fig. 4a, one can see three strong peaks of SnO_2 of (110), (101) and (211) crystal planes, besides, there are three strong peaks at $2\theta = 43.25°$, 50.4°, 74.05°, belong to the diffraction of

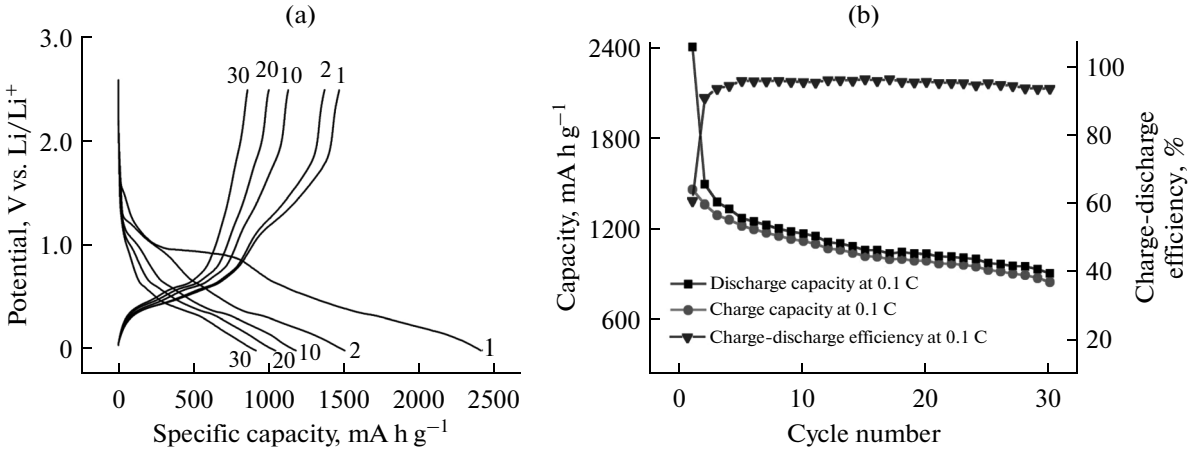

Fig. 5. (a) discharge/charge curves of the SnO_2 nano cuboids at 0.1 C rate; (b) cycle performance of the SnO_2 nano cuboids tested at 0.1 C for 30 cycles.

copper foil of (111), (200) and (220) crystal planes, which is confirmed by a comparison with the standard values (JCPDS 04-0836) presented in Fig. 4b. The other peaks of SnO_2 were not shown due to the strong diffraction of copper covering the peaks of SnO_2. The results showed that the organic substance didn't influence the structure of SnO_2. The sample in Fig. 4c was obtained by disassembled the anode after 16 cycles in a glove box, washed in acetone and dried in vacuum for 6 h. The XRD patterns in Fig. 4c show that the tin is the main components of the material, and most of tetragonal rutile SnO_2 essentially disappeared and turned to metallic Sn. The diffraction peaks in XRD patterns can be well indexed with the tetragonal phase of Sn, which is confirmed by a comparison with the standard values (JCPDS 65-0296) in Fig. 4d. In addition, the small peaks marked (*) of $2\theta = 29.9°$, 33.4°, 37.2°, 57.4° belong to tetragonal SnO (JCPDS 85-0423) and weak peaks marked (●) of $2\theta = 26.6°$, 33.9°, 37.9°, 51.8° belong to tetragonal SnO_2 (JCPDS 41-1445), which are derived from the reactions Eqs. (4), (5) and the reversible reaction Eq. (1). There are some amorphous peaks between $2\theta = 10°–30°$, which are attributed to the SEI components and amorphous Li_xSn alloys. While, in the XRD patterns, Li_2O was not observed, which maybe because the content is very little.

Galvanostatic discharge–charge tests have been carried out in the potential window of 0–2.5 V at a rate of 0.1 C for 30 cycles to evaluate the electrochemical performance of cuboid SnO_2 nanoparticles. Figure 5a shows the discharge/charge curves for the 1st, 2nd, 10th, 20th and 30th cycles of the SnO_2 nano-cuboids at 0.1 C rate; and Fig. 5b shows the cycle performance of the SnO_2 nano-cuboids tested at 0.1 C. In the first discharge profile, there is a voltage plateau at around 0.95 V due to the irreversible SEI formation, which disappears after the second charge–discharge cycle. The first discharge and charge capacities were 2410 and 1468 mA h g^{-1}, respectively, with coulombic efficiency of 60.9%. Obviously, the initial higher capacity is attributed to the conversion reaction (SnO_2–Sn) along with the alloy (Li_xSn) reaction of SnO_2 anode. The values are much higher than previously reported that 1520 and 742 mA h g^{-1} with coulombic efficiency of 48.8% for porous SnO_2 nano-spheres [32], 1673 and 815 mA h g^{-1} with coulombic efficiency about 48.7% for flowerlikeSnO_2 nanorod bundles [33], and 1790 and 750 mA h g^{-1} with coulombic efficiency of 41.8% for porous SnO_2 micro-tubes [34], 2105 and 1029 mA h g^{-1} for SnO_2 hollow nanospheres [35]. Generally accepted point is the formation of metallic Sn by the partially irreversible Eq. (1) and the formation of SEI film (Eq. (2)) by decomposition of solvent molecules and electrolyte solution, which in turn leads to consumption of excess amount of lithium and should be responsible for the first charge and discharge mismatch [4–6, 19–23]. That is the cathodic (discharge) capacity is the sum of reversible and irreversible capacity, and anodic (charge) capacity is a reversible capacity.

The second discharge and charge capacities of SnO_2 electrode are 1504 and 1370 mA h g^{-1}, respectively, with the coulombic efficiency was increased from 60.9% (first cycle) to 91.1%. After 20 cycles, it was found that the reversible discharge capacity of SnO_2 was still maintained at 1043 mA h g^{-1}, which is 1.97 times of that 530 mA h g^{-1} of porous SnO_2 microtubes [34]. After 30 cycles, it was found that the reversible discharge capacity of SnO_2 was still maintained at 915 mA h g^{-1} as showed in Fig. 5b, with the coulombic efficiency of 93.84%, which is 1.75 times of that of 522 mA h g^{-1} of porous SnO_2 nanospheres [32], and 2.46 times, of the theoretical capacity of graphite. Obviously, the discharge capacities keep at 1043 mA h g^{-1} after 20 cycles and 915 mA h g^{-1} after 30 cycles, which are larger than the theoretical capacity 782 mA h g^{-1} (corresponds to Li_xSn alloying-dealloying). So, the

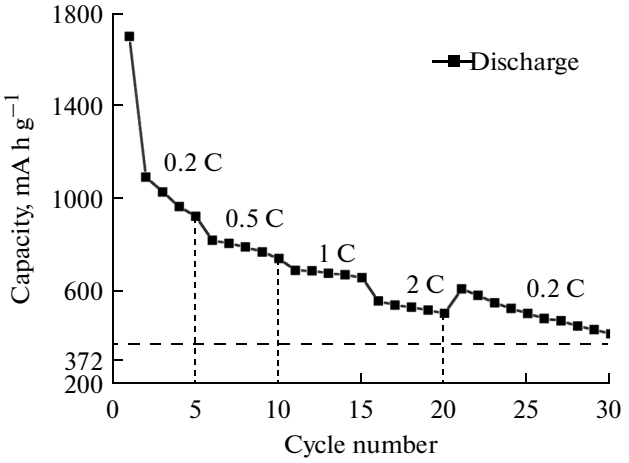

Fig. 6. Discharge capacities of the cuboid SnO_2 nanoparticles at different rates.

SnO_2 anode mechanism is the conversion reaction (of SnO_2–Sn–SnO–SnO_2) along with the alloy (Li_xSn) reaction.

It is worth noting that we used the same reagents and synthesis method as that in reference [34], the nano-cuboid SnO_2 was obtained in this study and the swallow tail like SnO_2 micro-tube was obtained in reference [34]. The differences in size and morphology of the two samples are attributed to the control of heat rate of the decomposition of $Sn_2C_2O_4$. In [34], the heat rate is very slow (1°C/min) and the CO_2 gas released slowly, resulted the SnO_2 particles grew larger and the release of CO_2 gas forming the tube. While in this study, the heat rate is fast (3°C/min), and the CO_2 gas released quickly and SnO_2 particles have no time to grow larger and forming the tube.

The discharge and charge capacities and coulombic efficiency obtained in this study (the initial values of 2410 and 1468 mA h g^{-1} with coulombic efficiency of 60.9%; the values after 20 cycles at 0.1 C still maintained at 1043 and 1000 mA h g^{-1} with coulombic efficiency of 95.9%) are higher than that in [34] (the initial values of 1790 and 750 mA h g^{-1} with coulombic efficiency of 41.8%; the values after 20 cycles at 0.1 C only maintained at 530 and 505 mA h g^{-1} with coulombic efficiency of 95.2%). This may be associated with that the size of cuboid SnO_2 in this study is about 40 nm in width, 100 nm in length and only about 10 nm in height. While the swallow tail like SnO_2 micro-tube is about 30 μm in length and 10 μm in diameter, and the much larger SnO_2 size is unfavorable to the electrochemical performance though the tube structure is favorable. The formed nanosized metallic Sn particles from nano-cuboid SnO_2 with enormous surfaces is believed to enhance the electrochemical activity towards the formation/deformation of Li_2O, which effectively enhanced the Li storage capacity. So the orientation is to control synthesis of SnO_2 with specific morphology and the nano-size particles, and resulted larger electrode specific surface area.

Cycle performances of SnO_2 was further investigated at different charge–discharge current densities of 0.2, 0.5, 1, 2 and 0.2 C (Fig. 6). The SnO_2 exhibits superior cycle stability and has higher Li^+ storage capacity (506 mA h g^{-1}) even at 2 C. After 30 cycles at different current densities, the reversible discharge capacity of SnO_2 was still maintained at 418 mA h g^{-1}, which is higher than that of graphite (372 mA h g^{-1}) and previously reported about 100 mA h g^{-1} of SnO_2 nanorods [36] and flower like SnO_2 [37].

4. CONCLUSIONS

A novel cuboid SnO_2 nanoparticles as LIB anode was synthesized by a simple precipitate of $SnCl_2$ in oxalic acid and followed by temperature—controlled decomposition of $Sn_2C_2O_4$. The XRD of cycled anode materials and CV spectra of the cell verified the reaction mechanism of SnO_2 anode is the conversion reaction of SnO_2–Sn–SnO–SnO_2 along with alloying reaction of Li_xSn. The electrochemical performance tests show that the initial discharge and charge capacity of cuboid SnO_2 nanoparticles are 2410 and 1468 mA h g^{-1} at the current density of 0.1 C, respectively. After 30 cycles at different current densities of 0.2, 0.5, 1, 2 and 0.2 C, the reversible discharge capacity is still maintained at 418 mA h g^{-1}, which indicates that the prepared cuboid SnO_2 nanoparticles exhibit a superior lithium capacity and cycle performance. The nanosize of SnO_2 is the main contribution of the high reversible charge and discharge capacities. All the results indicate the nano-cuboid SnO_2 has promising perspective as anode of LIB for its large reversible capacity, excellent cyclic performance and good rate capability.

ACKNOWLEDGMENTS

This study was financially supported by Guangdong Nature Science Foundation (S2011010005788) and the project of the scientific research conditions in Guangzhou (no. 2013-163-7).

REFERENCES

1. Wang, C., Zhou, Y., Ge, M., Xu, X., Zhang, Z., and Jiang, J.Z., *J. Am. Chem. Soc.*, 2010, vol. 132, p. 46.
2. Park, M.S., Wang, G.X., Kang, Y.M., Wexler, D., Dou, S.X., and Liu, H.K., *Angew. Chem. Int. Ed.*, 2007, vol. 46, p. 750.
3. Idota, Y., Kubota, T., Matsufuji, A., Maekawa, Y., and Miyasaka, T., *Science*, 1997, vol. 276, p. 1395.
4. Li, L.M., Yin, M., Liu, S., Wang, Y.G., Chen, L.B., and Wang, T.H., *Electrochem. Commun.*, 2010, vol. 12, p. 1383.
5. Wang, C., Zhou, Y., Ge, M., Xu, X., Zhang, Z., and Jiang, J.Z., *J. Am. Chem. Soc.*, 2010, vol. 132, p. 46.

6. Lou, X.W., Wang, Y., Yuan, C, Lee, J.Y., and Archer, L.A., *Adv. Mater.*, 2006, vol. 18, p. 2325.
7. Park, M.S., Wang, G.X., Kang, Y.M., Wexler, D., Dou, S.X., and Liu, H.K., *Angew. Chem. Int. Ed.*, 2007, vol. 46, p. 750.
8. Ma, X.L., Li, Y., and Zhu, Y.L., *Chem. Phys. Lett.*, 2003, vol. 376, p. 794.
9. Cheng, B., Russell, J.M., Shi, W., Zhang, L., and Samulski, E.T., *J. Am. Chem. Soc.,* 2004, vol. 126, p. 5972.
10. Yang, R., Gu, Y.G., Li, Y.Q., Zheng, J., and Li, X.G., *Acta Mater.*, 2010, vol. 58, p. 866.
11. Besenhard, J.O., Yang, J., and Winter, M., *J. Power Sources*, 1997, vol. 68, p. 87.
12. Brousse, T., Retoux, R., Herterich, U., and Schleich, D.M., *J. Electrochem. Soc.*, 1998, vol. 145, p. 1.
13. Nama, S., Kim, S., Wi, S., Choi, H., Byun, S., Choi, S.M., Yoo, S.I., Lee, K.T., Park, B., *J. Power Sources*, 2012, vol. 211, p. 154.
14. Wang, Y., Lee, J.Y., and Deivaraj, T.C., *J. Electrochem. Soc.*, 2004, vol. 151, p. A1804.
15. Larcher, D., Beattie, S., Morcrette, M., Edstrom, K., Jumas, J.C., and Tarascon, J.M., *J. Mater. Chem.*, 2007, vol. 17, p. 3759.
16. Liu, W.F., Huang, X.J., Wang, Z.X., Li, H., and Chen, L.Q., *J. Electrochem. Soc.*, 1998, vol. 145, p. 59.
17. Courtney, I.A. and Dahn, J.R., *J. Electrochem. Soc.*, 1997, vol. 144, p. 2045.
18. Brousse, T., Retoux, R., Herterich, U., and Schleich, D.M., *J. Electrochem. Soc.*, 1998, vol. 145, p. 1.
19. Larcher, D., Beattie, S., Morcrette, M., Edstrom, K., Jumas, J.C., and Tarascon, J.M., *J. Mater. Chem.*, 2007, vol. 17, p. 3759.
20. Wang, H.E., Xi, L.J., Ma, R.G., Lu, Z.G., Chung, C.Y., Bello, I., and Zapien, J.A., *J. Solid State Chem.*, 2012, vol. 190, p. 104.
21. Aravindan, V., Jinesh, K.B., Prabhakar, R.R., Kale, V.S., and Madhavi, S., *Nano Energy*, 2013, vol. 2, p. 720.
22. Choi, N.S., Yao, Y., Cui, Y., and Cho, J., *J. Mater. Chem.*, 2011, vol. 21, p. 9825.
23. Guo, X.W., Fang, X.P., Sun, Y., Shen, L.Y., Wang, Z.X., and Chen, L.Q., *J. Power Sources*, 2013, vol. 226, p. 75.
24. Kilibarda, G., Szabó, D.V., Schlabach, S., Winkler, V., Bruns, M., and Hanemann, T., *J. Power Sources*, 2013, vol. 233, p. 139.
25. Wachtler, M., Besenhard, J.O., and Winter, M., *J. Power Sources*, 2001, vol. 94, p. 189.
26. Li, J.T., Chen, S.R., Fan, X.Y., Huang, L., and Sun, S.G., *Langmuir*, 2007, vol. 23, p. 13174.
27. Lucas, I.T., Pollak, E., and Kostecki, R., *Electrochem. Commun.*, 2009, vol. 11, p. 2157.
28. Lian, P.C., Zhu, X.F., Liang, S.Z., Li, Z., Yang, W.S., and Wang, H.H., *Electrochim. Acta*, 2011, vol. 56, p. 4532.
29. Yao, J., Shen, X., Wang, B., Liu, H., and Wang, G., *Electrochem. Commun.*, 2009, vol. 11, p. 1849.
30. Cheng, J.L., Xin, H.L., Zheng, H.M., and Wang, B., *J. Power Sources*, 2013, vol. 232, p. 152.
31. Zhang, X., Liang, J., Gao, G., Ding, S., Yang, Z., Yu, W., and Li, B.Q., *Electrochim. Acta*, 2013, http://dx.doi.Org/10.1016/j.electacta.2013.03.036.
32. Wen, Z.G., Zheng, F., and Liu, K.L., *Mater. Lett.*, 2012, vol. 68, p. 469.
33. Wen, Z.G., Zheng, F., Yu, H.C., Jiang, Z.R., and Liu, K.L., *Mater. Charact.*, 2013, vol. 76, p. 1.
34. Xu, M.W., Zhao, M.S., Wang, F., Guan, W., Yang, S., and Song, X.P., *Mater. Lett.*, 2010, vol. 64, p. 921.
35. Kim, W.S., Hwa, Y., Jeun, J.H., Sohn, H.J., and Hong, S.H., *J. Power Sources*, 2013, vol. 225, p. 108.
36. Liu, H.D., Huang, J.M., Li, X.L., Liu, J., and Zhang, Y.X., *Ceram. Int.*, 2012, vol. 38, p. 5145.
37. Liu, H.D., Huang, J.M., Li, X.L., Liu, J., Zhang, Y.X., and Du, K., *Appl. Surf. Sci.*, 2012, vol. 258, p. 4917.